REPORT DOCUMENTATION PAGE

Form Approved
OMB No. 0704-0188

1. REPORT DATE *(DD-MM-YYYY)*	**2. REPORT TYPE**	**3. DATES COVERED** *(From - To)*
12-10-2009	Final Report	15 Feb 2008-31 Mar 2009

4. TITLE AND SUBTITLE

NittanySat Final Report for University Nanosatellite-5 Program

5a. CONTRACT NUMBER
FA9550-07-1-0190

5b. GRANT NUMBER

5c. PROGRAM ELEMENT NUMBER

6. AUTHOR(S)

Adam C. Escobar, Sven G. Bilén, Robert M. Capuro

5d. PROJECT NUMBER

5e. TASK NUMBER

5f. WORK UNIT NUMBER

7. PERFORMING ORGANIZATION NAME(S) AND ADDRESS(ES)

Pennsylvania State University
110 Technology Center
University Park, PA 16802-
1003

8. PERFORMING ORGANIZATION REPORT NUMBER

N/A

9. SPONSORING / MONITORING AGENCY NAME(S) AND ADDRESS(ES)

AFOSR
4015 Wilson Blvd
Arlington, VA 22203-1954

10. SPONSOR/MONITOR'S ACRONYM(S)

11. SPONSOR/MONITOR'S REPORT NUMBER(S)

12. DISTRIBUTION / AVAILABILITY STATEMENT A

13. SUPPLEMENTARY NOTES

14. ABSTRACT

The NittanySat team has completed the Flight Competition Review (FCR), which marks the culmination of the 2-year development of a prototype of a nanosatellite as part of the University NanoSat-5 Program. At this review, entries from ten universities were judged on their mission relevance and payload readiness. From the over 60 students on the NittanySat team, seven students attended the FCR, which was held outside of Kirtland Air Force Base. NittanySat was not selected for flight; however, the students learned the hands-on and practical design techniques for the development of a nanosatellite.

The NittanySat mission was to investigate the high-latitude *D*-region of the ionosphere and its effects on radio frequency communications. The *D*-region variability would have been studied by measuring radio wave absorption and scintillation caused by the enhanced ionization from energetic particles and plasma irregularities.

15. SUBJECT TERMS

16. SECURITY CLASSIFICATION OF:			**17. LIMITATION OF ABSTRACT**	**18. NUMBER OF PAGES**	**19a. NAME OF RESPONSIBLE PERSON**
a. REPORT	**b. ABSTRACT**	**c. THIS PAGE**		15	**19b. TELEPHONE NUMBER** *(include area code)*

Standard Form 298 (Rev. 8-98)
Prescribed by ANSI Std. Z39.18

TABLE OF CONTENTS

1.0 Objectives

1.1 Mission Statement

NittanySat will investigate the high-latitude *D*-region of the ionosphere and its effects on radio frequency communications. The *D*-region variability will be studied by measuring radio wave absorption and scintillation caused by the enhanced ionization from energetic particles and plasma irregularities.

1.2 Mission Objectives

- Measure the amplitude and variability of the radio wave absorption at several HF wavelengths (Mission Step 4a).
- Measure the amplitude and locations of the scintillations on radio frequencies (Mission Step 4a).
- Correlate the absorption and scintillation effects on RF communications with energetic particle flux and local plasma environment (Mission Step 4b and 4c).
- Calibrate high latitude ground-based imaging riometers.

2.0 Status of Effort

The NittanySat team has completed the two-year development of a nanosatellite, starting with the proposal and ending with a proto-nanosatellite. The flight competition review (FCR) marked the conclusion of the project. At this review, ten universities presented their nanosatellite projects, where only one school was provided the opportunity for an orbital launch. NittanySat was not selected; however, the students learned the hands-on and practical design techniques for the development of a nanosatellite.

The students have developed many prototypes for the various sub-systems. We finished with a student work force of approximately 60 students and 5 faculty advisors. The students involved range from first-year to graduate level in many disciplines: electrical engineering, aerospace engineering, mechanical engineering, civil engineering, physics, and computer science and engineering. Five electrical and aerospace engineering faculty act as the advisors to this project assisting in educating the next generation of engineers. NittanySat also has international and domestic collaboration with the University of Graz in Austria, the University of Tromsø in Norway, and the University of Alaska at Fairbanks.

The FCR took place outside of Kirtland Air Force Base, where seven students traveled to present several demonstrations for NittanySat. The demonstrations included presentations of the payload science instruments, communications, attitude determination instruments, power systems, and the antenna deployment system. The effort put into developing NittanySat is important because the lessons learned from this project will be handed down to future missions.

3.0 Accomplishments/New Findings

3.1 Mission Management

3.1.1 Mission Success Criteria

Minimum Success Criteria

1. Operate in a near-polar orbit between an altitude of 400 km and 1000 km with an inclination of at least 65°.
2. Two-way communication with the flight system and the ground station at Penn State.
3. Achieve gravity gradient stable satellite configuration with *z*-axis pointing within ±20° of nadir.
4. Collect and download HF absorption data from at least one orbital pass over a polar ground station with data download at Penn State.

Comprehensive Success Criteria

1. Operate in a near-polar orbit between an altitude of 400 km and 800 km with an inclination of at least 70°.
2. Measure the local plasma environment and energy flux during overpasses.
3. Collect at least 6 sets of data each day with at least 3 sets during the first 12 hours of the day and the last 3 sets during the last 12 hours of the day.
4. Gather data in an intense operation mode for disturbances with $Kp > 6$.
5. Operate at least two high latitude stations in addition to a command and control data station at Penn State.

3.1.2 Concept of Operations

Mission Initialization Phase

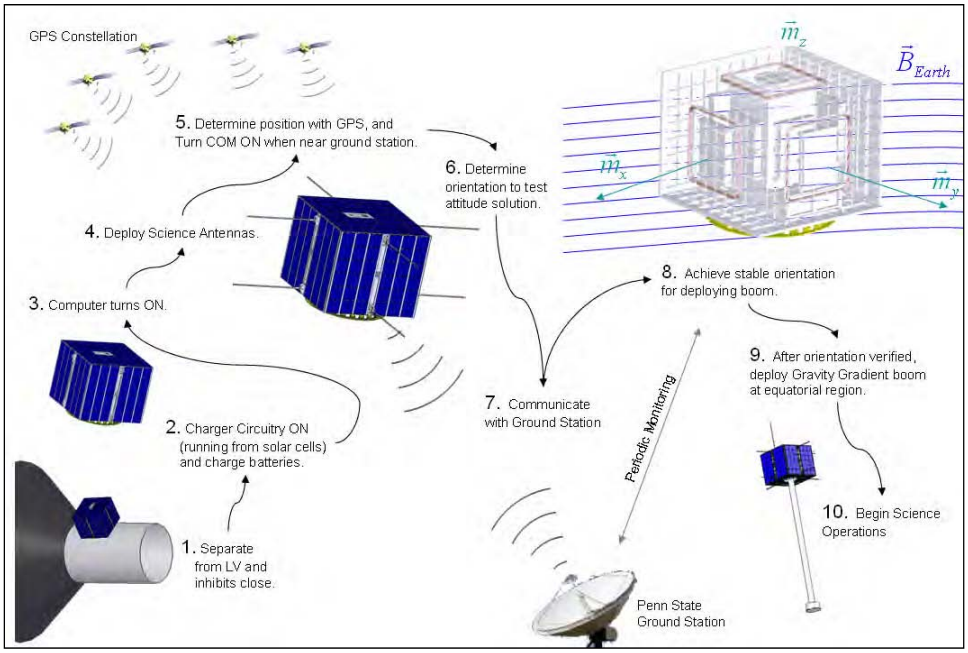

Figure 1 - Mission Initialization Concept of Operations

Science Mission Phase

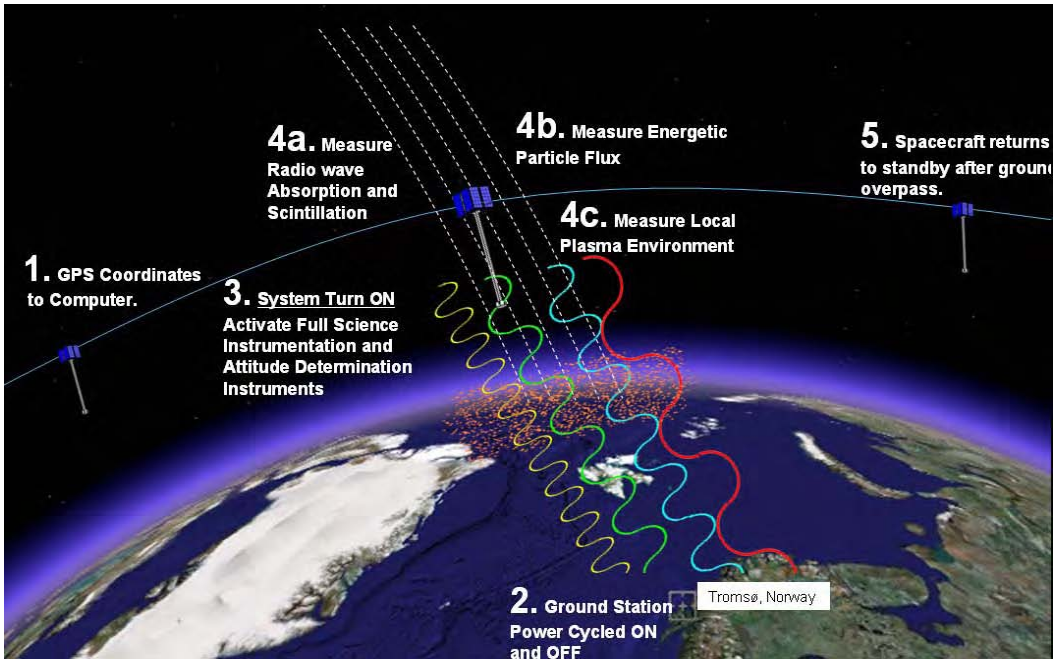

Figure 2 - Mission Science Concept of Operations. Numbers correspond to mission objectives.

3.1.3 Educational Goals

NittanySat aims to educate the next generation of engineers. The project has a workforce from all skill levels from first-year to graduate students. The primary goal is to teach these students practical design techniques not taught in the classroom. NittanySat is also involved in outreach events for younger students from K–12. The goal is to get students interested in the space sciences and engineering.

3.2 RF Absorption Experiment

The RF Absorption Experiment (ABEX) consists of a transmitter and receiver. The transmitter is located on the ground, and the receiver is part of the flight system. The reason for this configuration is due to the limitation of power on the flight system. In order to determine radio-wave absorption, multiple frequencies need to be employed. The relative loss of power between radio waves determines the *D*-region absorption due to the collision frequency and electron density of this region. The mid to upper HF bands experience the most absorption and, therefore, have been chosen to be used for this science investigation.

Scintillation is the second radio-wave alteration that will be monitored. The scintillation data will be compared with the other science instrument data in order to determine any relationships. Scintillations affect two properties of a radio-wave: amplitude and phase. The scope of NittanySat's science goals only requires the amplitude of the radio wave to be tracked. Tracking the phase variations will add more complexity to the design of the ABEX instrument. The indices of scintillation and power spectral density plots will be found to compare with the science phenomena.

Since the science mission is to investigate the high latitude ionosphere, the ground-based transmitters will be stationed in the auroral regions. Currently there are two universities that will collaborate and operate these stations: the University of Alaska at Fairbanks (transmit site will actually be at Poker Flat, Alaska) and the University of Tromsø in Norway. The University of Graz in Austria is another collaborator that has assisted in the design of the flight system receiver.

3.2.1 ABEX Interface Diagram

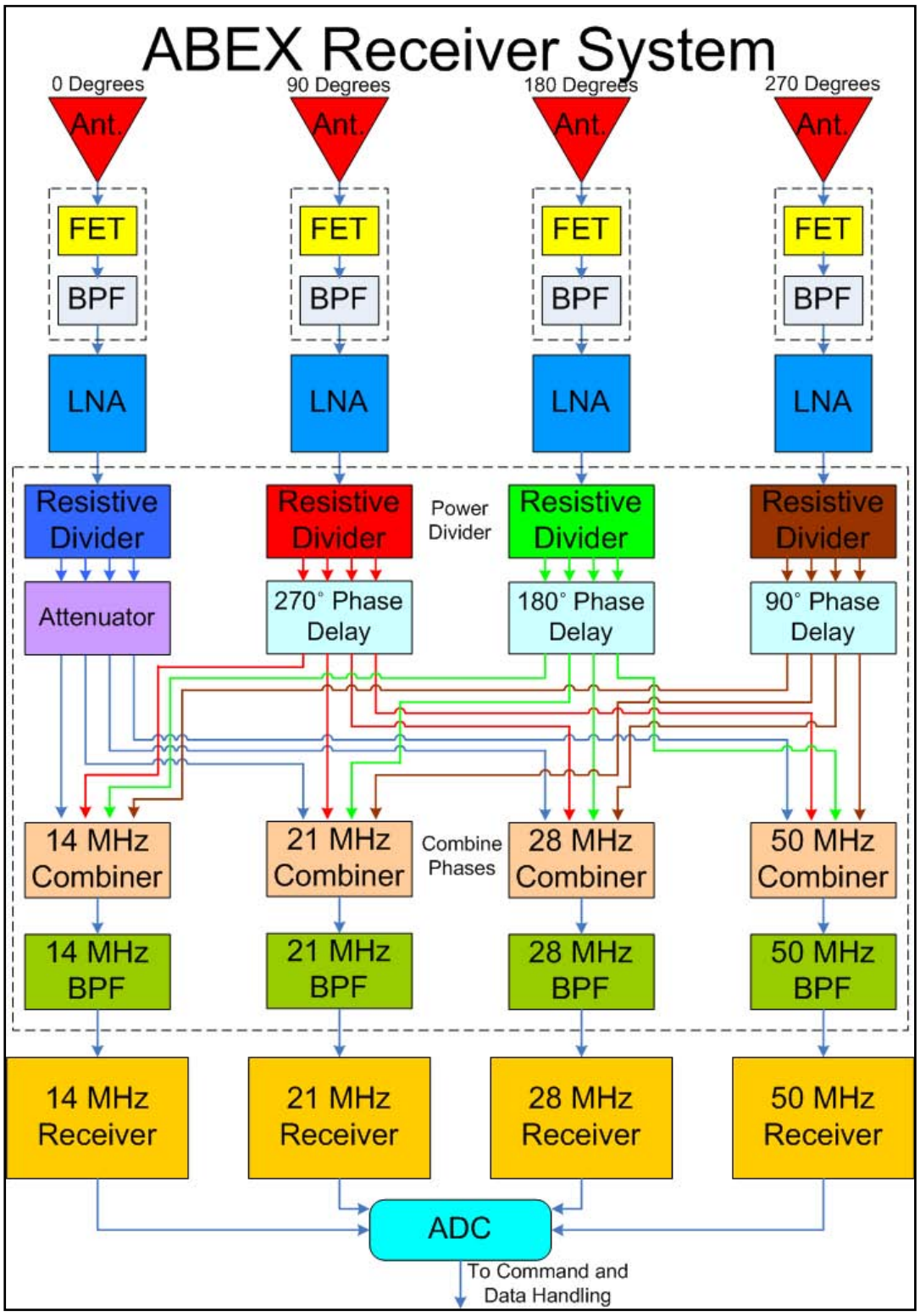

Figure 3 - ABEX Electrical Interface Diagram.

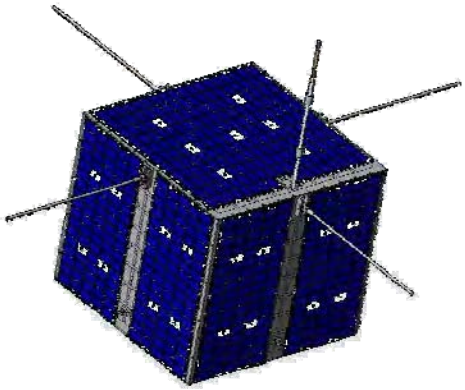

Figure 4 - NittanySat with ABEX antennas and Langmuir probe deployed.

The receive system contains four monopoles mounted orthogonal to each other on the +z-face of the payload. Figure 4 illustrates the four short monopoles (16 in. in length) mounted to the structure. The fifth element perpendicular to the plane of the 4 monopoles is the boom and probe for the Langmuir probe experiment. Figure 3 depicts the detailed electrical interface diagram. Each monopole is fed to active antenna circuitry, which includes a cascaded field effect transistor (FET) and a wideband band-pass filter. Next, there is a low noise amplifier (LNA), which increases the signal-noise-ratio. Since there are four frequencies of interest, the signal from each monopole needs to be divided into four separate signals. Next, since each monopole is out of phase by 90 degrees, phase shifters are required to allow all signals to add in phase prior to the receiver. There is an attenuator on the 0 degree path, because the signal amplitude needs to be equal prior to addition for each monopole. After the phase delay stage, there are four combiners corresponding to each receiver. Prior to the receivers, there are four narrow-band band-pass filters designed and tuned to the appropriate HF/VHF band center frequency. Each receiver measures the peak-to-peak voltage of the received signal, and outputs a 0–5 V signal to an analog-to-digital converter (ADC). The ADC digital data is input to the command and data handing (CDH) subsystem for data storage by the flight computer. Each receiver requires a matching network at the input. This was completed by a transformer plus RLC circuit.

3.2.2 ABEX Testing

Each component in the electrical interface diagram was tested. The LNAs, dividers, and combiners were procured, and the results are not presented here. The receivers already have flight history, which have flown on 12 sounding rocket missions. The results for this single component are not presented either. The previous components were to be tested during the instrument validation with the entire flight instrument assembled. The results presented are for the active antenna, wide band-pass filter, phase shifters, narrow band-pass filters, and receiver input matching network. Each component was first simulated using Microwave Office, and then manufactured and tested using either a spectrum analyzer or network analyzer.

Active Antenna Circuitry Test

A functionality test was completed for the active antenna circuitry. A spectrum analyzer, RF source, and antenna tuner were used for the test. Figure 5 depicts the test setup. The test was done in a "noisy" environment, where a lot of motors and rotating machinery are present in the vicinity. First, the noise floor was measured with the RF source OFF. Then the RF source was turned ON and the change in amplitude was measured. Figure 6 depicts the change in amplitude.

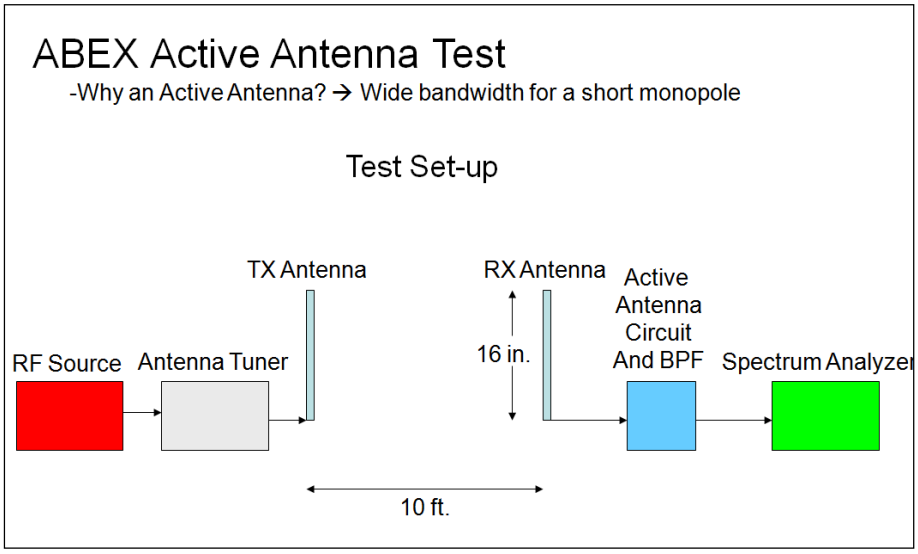

Figure 5 - ABEX active antenna setup.

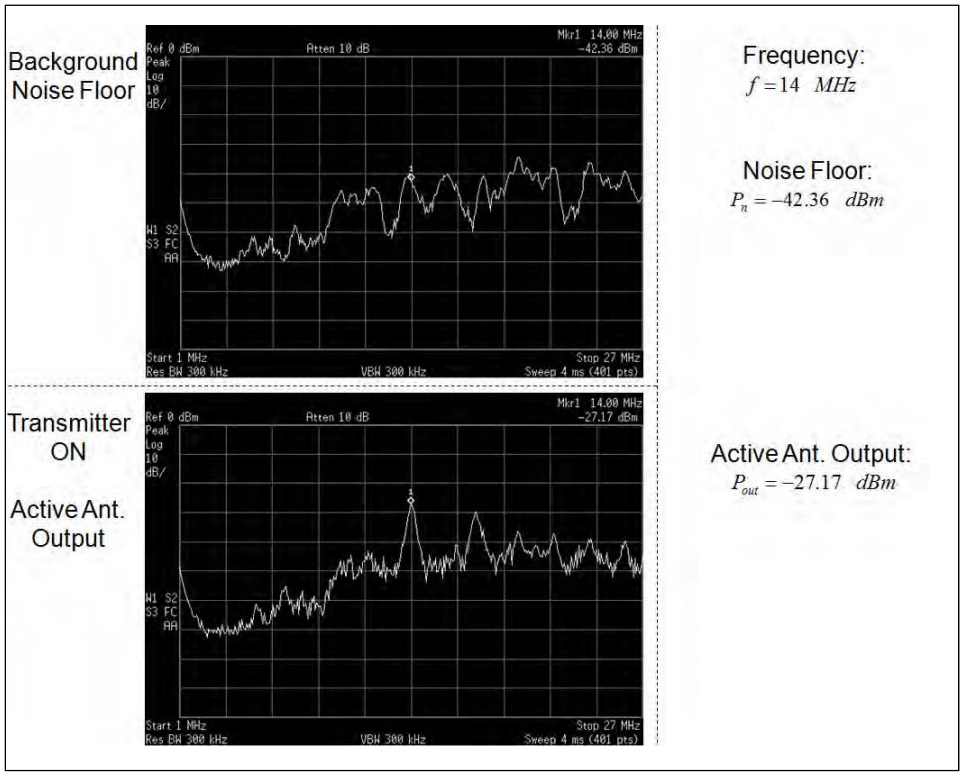

Figure 6 - Active antenna results viewed from a spectrum analyzer.

Wide Band-Pass Filter Test

The wide band-pass filter has a pass-band that includes all the four frequencies transmitted for the ABEX. The filter was tested with a network analyzer. Figure 7 includes 6 markers that index the frequencies of interest. The bandwidth (55.88 MHz) is marked by marker 5 and 6. Table 1 lists the insertion loss for each frequency of interest.

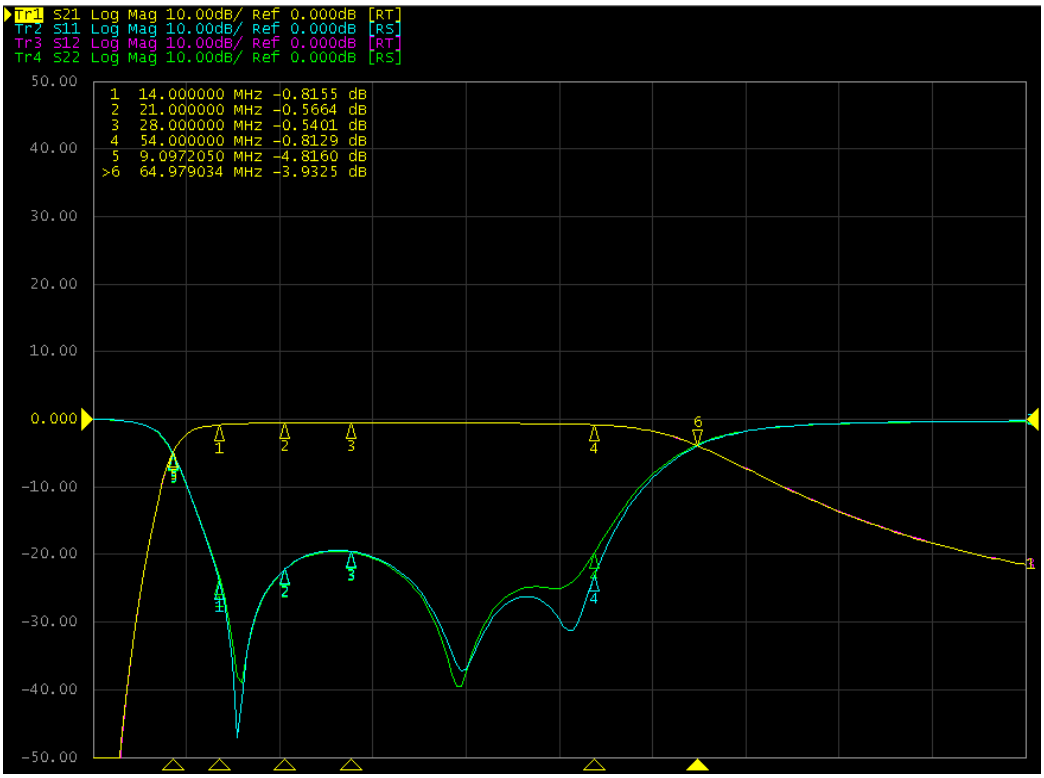

Figure 7 - S parameters of the wide band-pass filter.

Table 1 - Loss Associated with Frequency Band for 5 Pole Band-pass Filter

Frequency Band [MHz]	S_{21} [dB]
14	−0.82
21	−0.57
28	−.54
50	−0.81

Phase Shifters Test

A network analyzer was used to obtain the S parameters of the 90-degree phase shifter. Figure 8 depicts the S parameter data. The other two phase shifters display similar properties, except for greater phase delay.

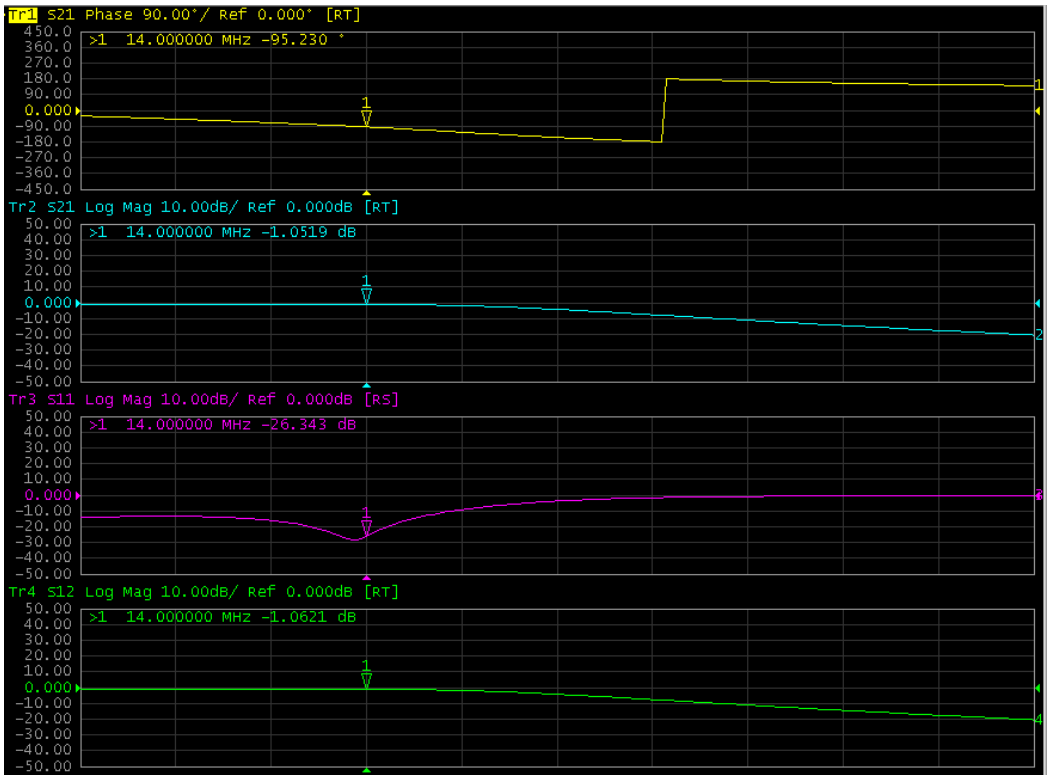

Figure 8 - S parameters for the 90-degree phase shifter.

Narrow Band-Pass Filters Test

The narrow band-pass filters test data are depicted in Figures 9 through 12 and tabulated in Table 2.

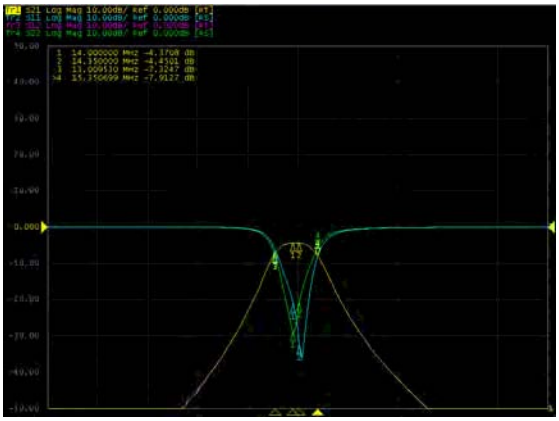

Figure 9 – 14-MHz BPF.

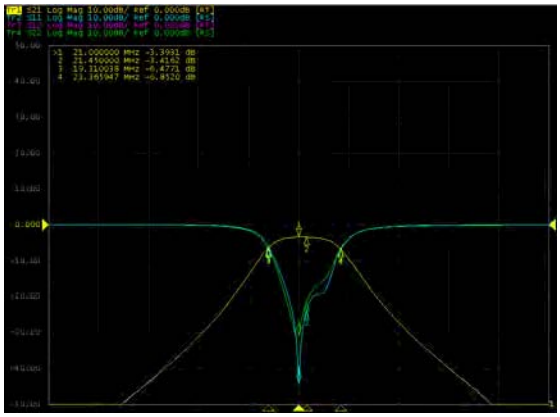

Figure 10 – 21-MHz BPF.

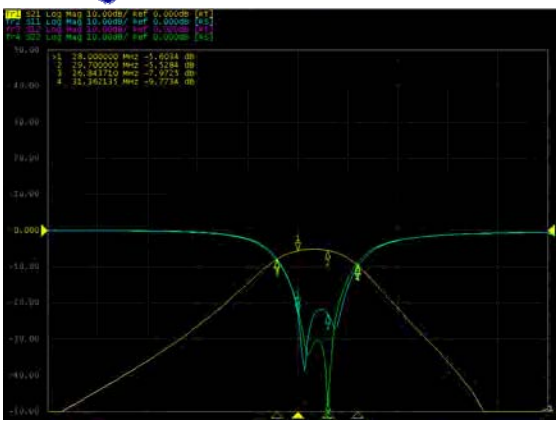

Figure 11 – 28-MHz BPF.

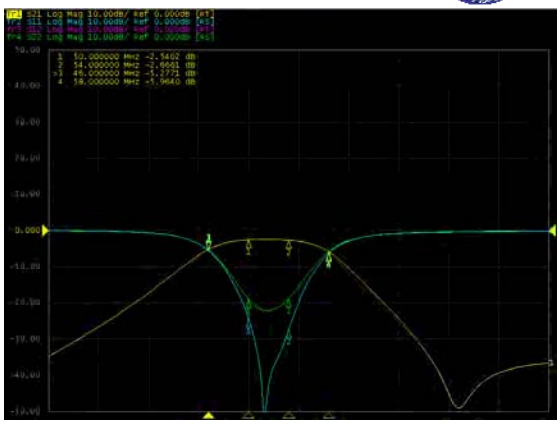

Figure 12 – 50-MHz BPF.

Table 2 - Narrow Band-pass Filter Parameters

Frequency Band [MHz]	Bandwidth Range [MHz]	Insertion Loss [dB]	Return Loss [dB]
14.0 – 14.35	13.0 – 15.35	−4.4	−34
21.0 – 21.45	19.3 – 23.37	−3.4	−43
28.0 – 29.7	26.84 – 31.36	−5.6	−38
50.0 – 54.0	46.0 – 58.0	−2.6	−55

Receiver Input Matching Test

The input impedance of the matching network was first found by a network analyzer finding the S_{11} parameter. With this information known, the necessary values for the components for the matching network were found. The results for the input matching network are depicted in Figures 13 through 21. The input matching is capable of being tuned over the entire range of the band.

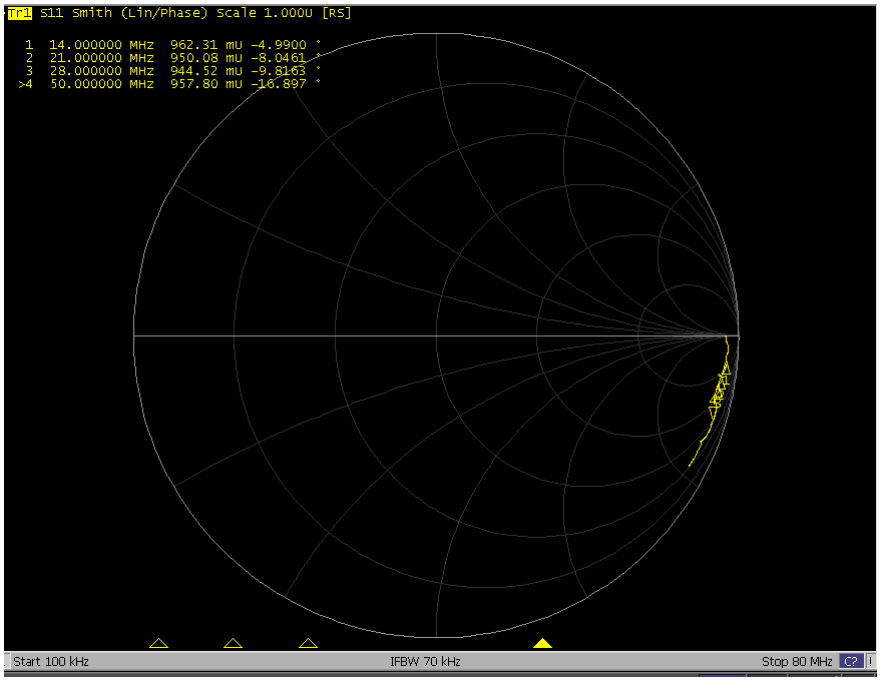

Figure 13 - Receiver input reflection coefficient without input matching network.

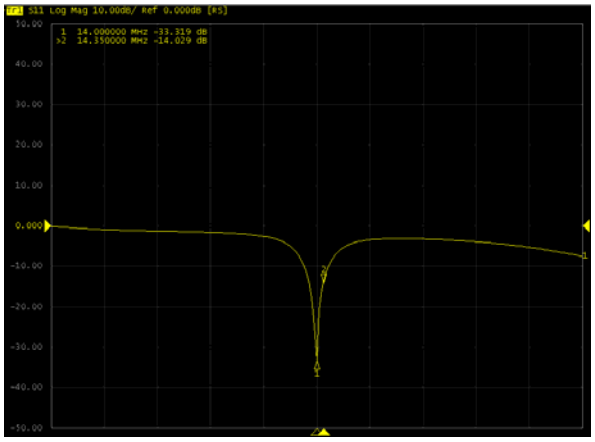

Figure 14 - Log/Mag plot of 14-MHz RX input matching.

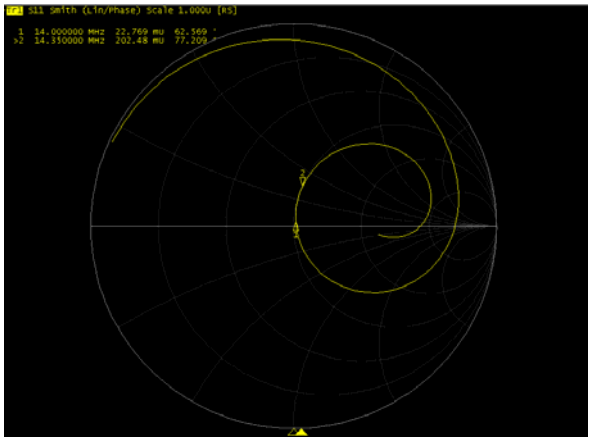

Figure 15 - Smith Chart of 14-MHz RX input matching.

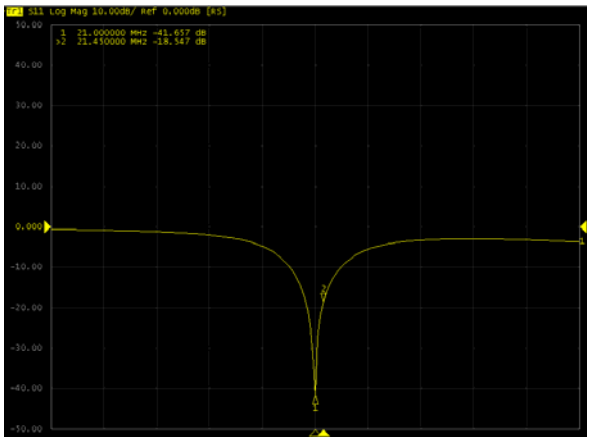

Figure 16 - Log/Mag plot of 21-MHz RX input matching.

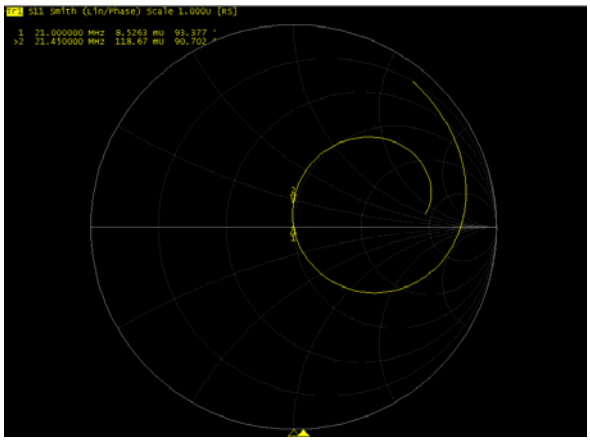

Figure 17 - Smith Chart of 21-MHz RX input matching.

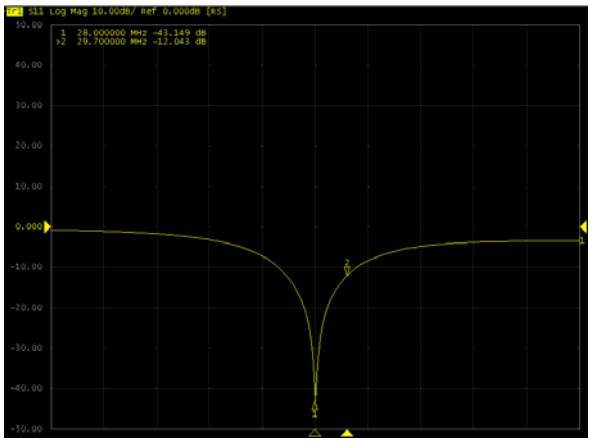

Figure 18 - Log/Mag plot of 28-MHz RX input matching.

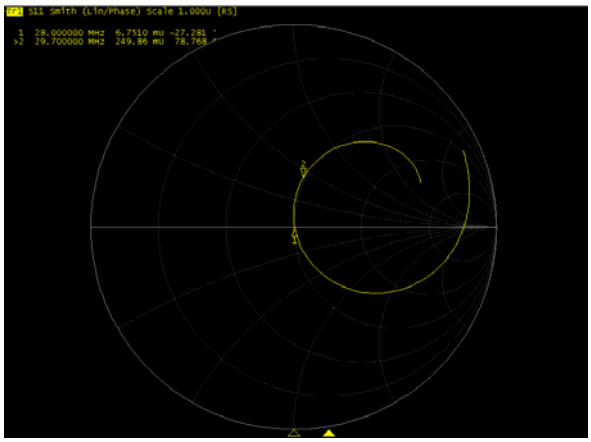

Figure 19 - Smith Chart of 28-MHz RX input matching.

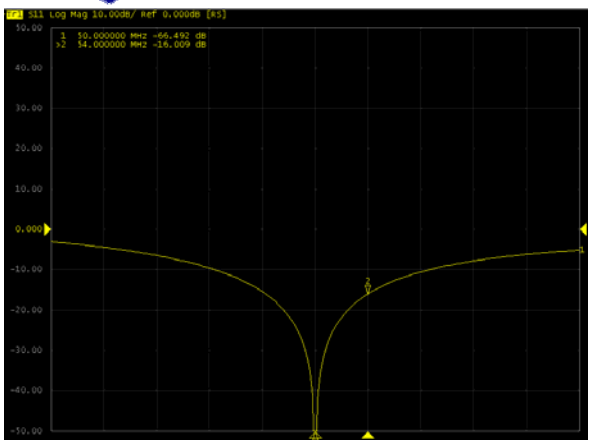

Figure 20 - Log/Mag plot of 50-MHz RX input matching.

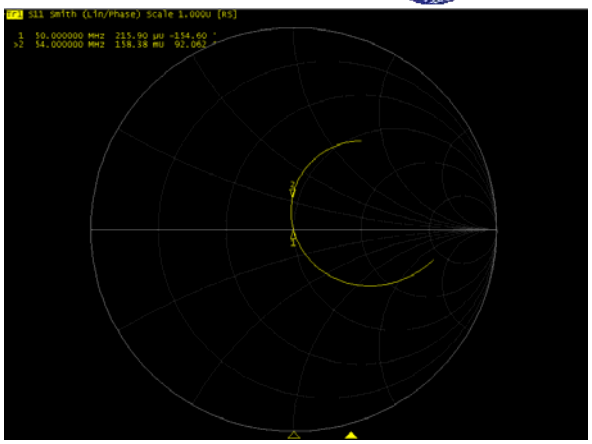

Figure 21 - Smith chart of 50-MHz RX input matching.

3.3 Energetic Particle Detector Experiment

The Energetic Particle Detector (EPD) Experiment measures the high energy electron and proton flux. These high energy electrons and protons are emitted from the sun through solar flares and coronal mass ejections. Once these particles come near Earth, the particles tend to follow the geomagnetic field and, therefore, the polar and auroral regions are the primary area for this particle precipitation. The energy of the particle and the number of collisions with the particles in the Earth's upper atmosphere will determine the penetration depth of the energetic particle. Low energy particles will tend to deposit in the upper ionosphere. The higher the energy of the particle, then the deeper the penetration. Therefore, the payload requirements stem from the science requirements that provide the range and resolution of the detectors to measure the energetic particles that reach the *D*-region. Knowing the ranges and resolutions of the energetic particles to be measured, the instrument specifications can be chosen. There will be two separate detectors; one will be to measure the energetic electron flux, and the second is to measure the energetic proton flux. The energetic particle detectors will be procured from Canberra.

No further work was completed after the CDR for the energetic particle detector due to limited personnel resources. Figure 22 displays the cross-section for the sensor head. The copper lining was used to reduce scattering, and the Mylar window was used to block sunlight from the sensor. Behind the sensor is the preamp board; then the signal goes to another set of circuitry for further signal conditioning and digital processing.

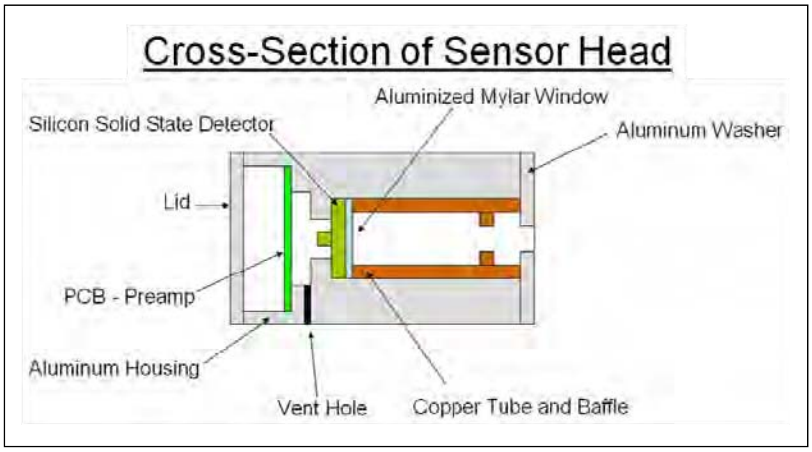

Figure 22 - Cross-section of the energetic particle detector sensor head.

3.4 Langmuir Probe Experiment

The Langmuir Probe Experiment (LP) will measure and monitor the local plasma environment. This would be the *F*-region of the ionosphere, and this experiment will monitor the variations between the quiet-time ionosphere with little to no energetic particle precipitation to an enhanced *F*-region due to the high energetic particle precipitation that causes a high *D*-region collision frequency, hence radio-wave absorption. The LP will measure the plasma potential, electron density, electron temperature, and positive ion density. This data will then be compared to the RF Absorption Experiment data and the Energetic Particle Detector Experiment data. The basic operation of the Langmuir Probe Experiment is to place a conductor at the end of a nonconductive boom and bias a voltage relative to the spacecraft. This bias voltage then collects a current that can be measured. The knowledge of this current–voltage relationship along with the probe geometry provides relationships to the surrounding plasma environment characteristics.

3.4.1 LP Interface Diagram

There are five components that comprise the Langmuir probe experiment: (1) the probe, (2) relay front end, (3) electrometer, (4) control and processing board, and (5) the power board. The instrument for NittanySat requires only one probe and the supporting circuitry for this probe. The LP experiment was developed for a M.S. thesis (Escobar, 2009), and this instrument was originally designed to support up to two probes. Figure 23 outlines the detailed electrical interface, and Figure 24 illustrates the mechanical interface diagram. There are only two elements necessary for the entire instrument. One circuit box houses the electrometers, relay board, and control and processing board, and the second circuit box contains the power regulation board. The circuit boxes are stacked upon each other, where a header interfaces the control and processing board and the power regulation board.

The electrometers are housed in their own enclosures within the first circuit box to mitigate any electromagnetic interference. The relay board was also enclosed in its own section for the same reason. The electrometers provide a logarithmic relationship and measures currents from tens of pico-amps to tens of micro-amps. The relay board switches between normal operation, electrometer calibration, and probe clean mode. For the electrometer calibration mode, glass encapsulated high resistance resistors are used to simulate the current to be measured. In the probe clean mode, a high voltage is applied on the probe in order for the free electrons to bombard the probe surface in order to remove contaminants.

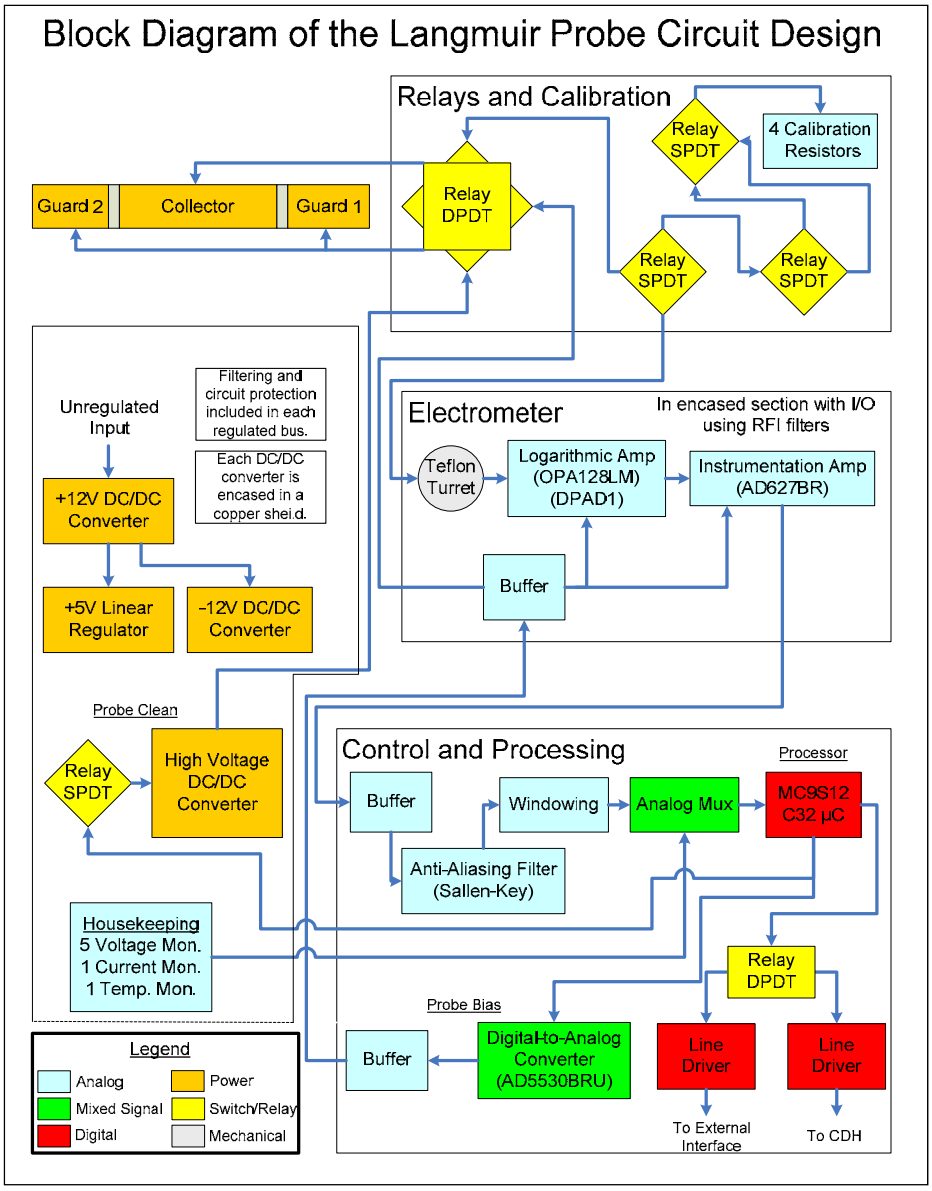

Figure 23 – LP internal electrical interface diagram.

The control and processing board is in the next compartment. This board provides the signal bias for the probe, signal conditioning, data sampling, and processor. The communication protocol can be selected to be either RS-232 or RS-422 depending on the mission requirements. Box 1 operates on three regulated voltages (+12 V, +5, and –12 V). These voltages can be supplied to the control and processing board directly, if the payload has these three voltages; therefore, the power regulation board would not be required for proper operation. If these voltages are not present, then the power regulation board is necessary. The power regulation board is capable of a 15 – 36.5 V input that is filtered by passive and active filters. This filters reduce the voltage ripple to less than 1 mV, and also does not contaminate the unregulated input supply bus.

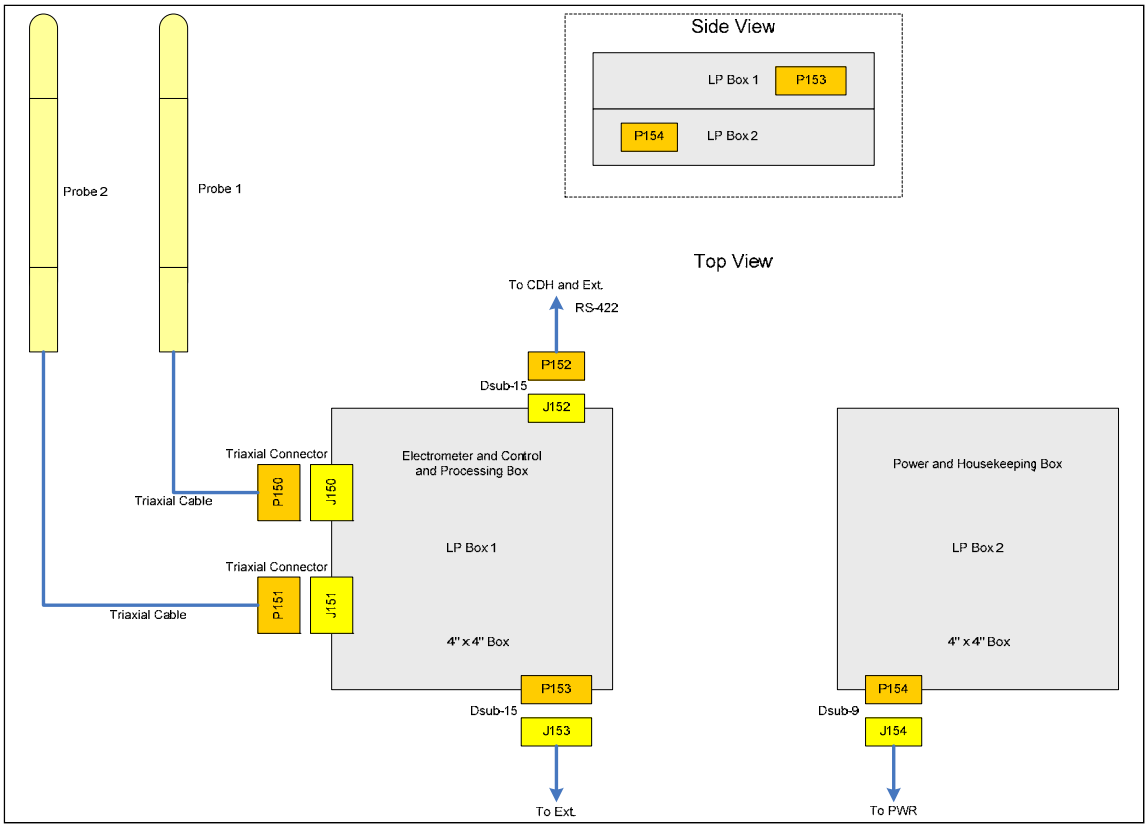

Figure 24 - Mechanical interface diagram with external electrical interfaces.

The probe was designed to operate using orbital-motion-limited theory. The radius of the probe is 1/16 in., which is small enough to function in all regions of the ionosphere. The probe contains three sections: the collector and two guards. The collector is in between the two guards separated by two thin Teflon washers. The probe is composed of brass, which is nickel and gold plated. The gold is the top layer that minimizes surface patchiness and the photoelectric effect. The nickel layer is required, because if gold was plated directly onto the brass, then the copper in the brass would diffuse into the gold layer. The copper in this layer would react to the atomic oxygen in the atmosphere, which creates a contaminant layer on the probe surface. Coating the probe with nickel mitigates this issue. Figure 25 displays the assembled probe. A triaxial cable provides the interface between the probe and the electrometer. The use of this cable reduces capacitance and isolates the signal from any electromagnetic interference. There is also a requirement that the probe has to be placed in an undisturbed region of plasma. A carbon fiber composite boom fulfills this requirement.

Figure 25 - Picture of Langmuir probe.

3.4.2 LP Testing

Each of the five components of the Langmuir probe experiment was tested; however, the entire instrument has not been validated. The instrument validation will occur once the plasma chamber is completed. The electrometer was tested by calibration with high resistance resistors in an encased metal box. Figure 26 shows this calibration enclosure. Figure 27 displays the calibration curve of the electrometer.

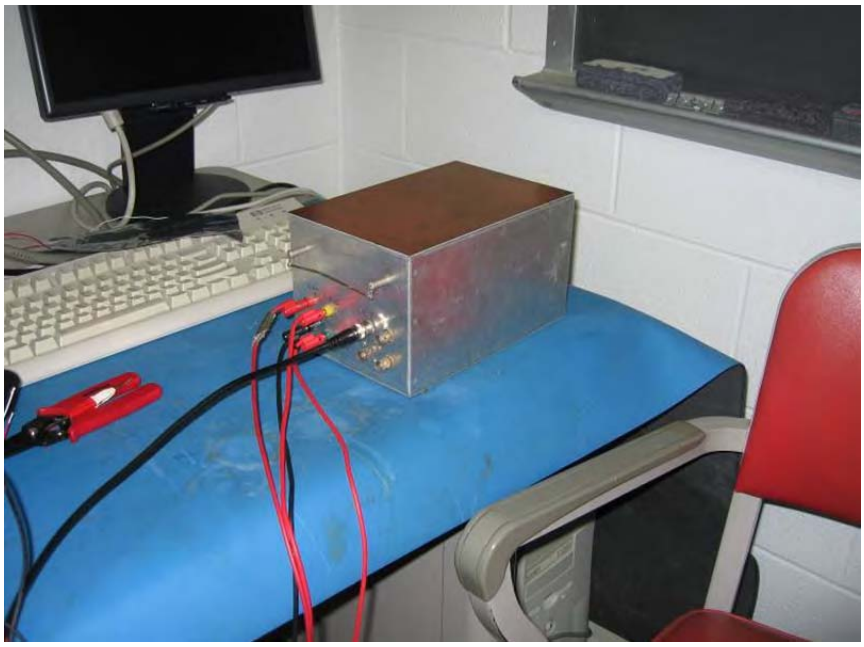

Figure 26 - Testing of the electrometer.

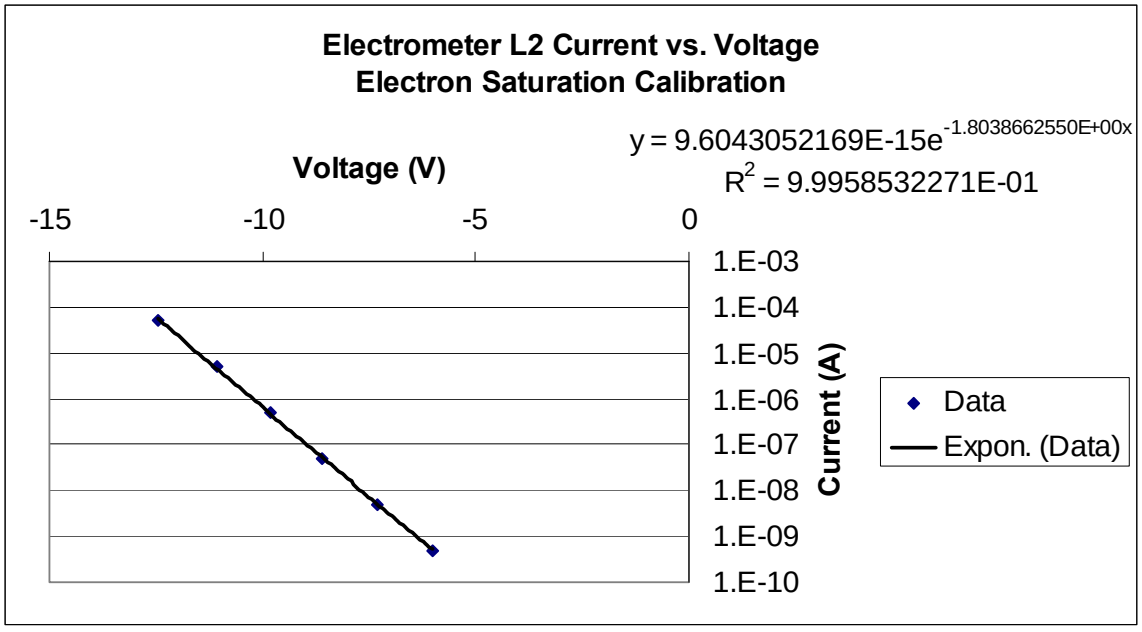

Figure 27 - Electrometer calibration data.

The next board tested was the control and processing board. All parts operated as intended. Figure 28 displays the sawtooth waveform bias, which was sent to the electrometer to bias the probe.

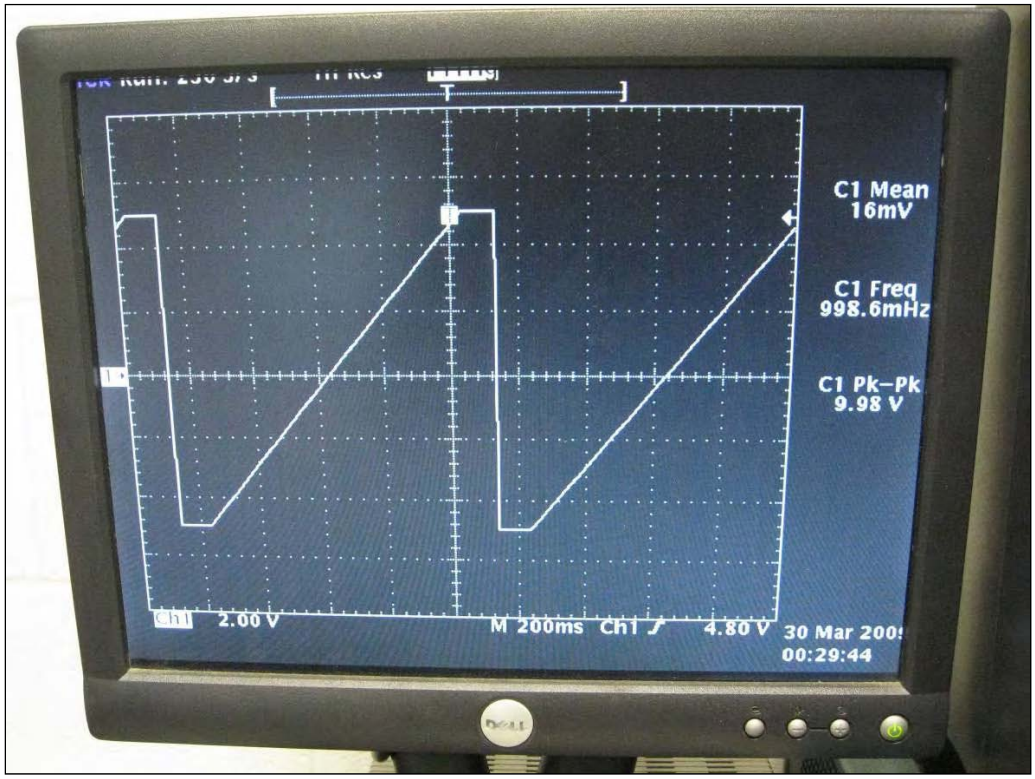

Figure 28 - Plot of LP swept voltage bias.

The last board to be tested is the power regulation board. Figures 29 through 36 below illustrate the effectiveness of the filtering. A spectrum analyzer measured the amount of power generated by the voltage ripple on the bus. The pictures on the left show the input, and the pictures on the right display the output of the +5 V bus. There is more improvement seen as each filtering stage has been added.

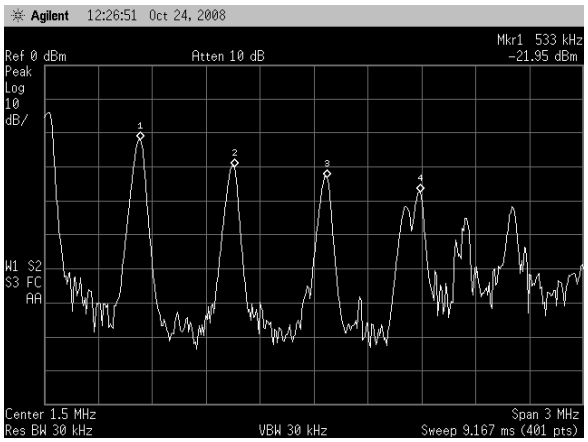

Figure 29 - Input with no filtering.

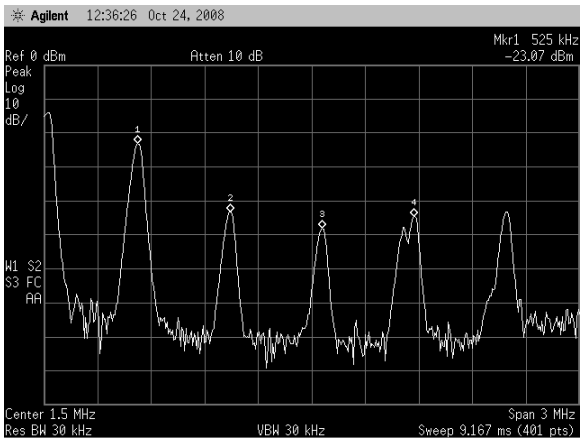

Figure 30 - Output with no filtering.

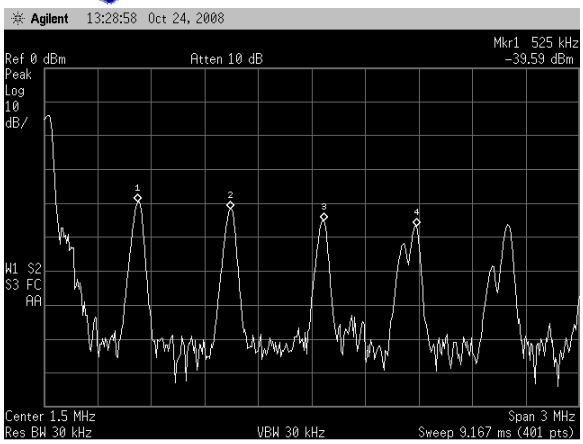

Figure 31 - Input with passive filtering.

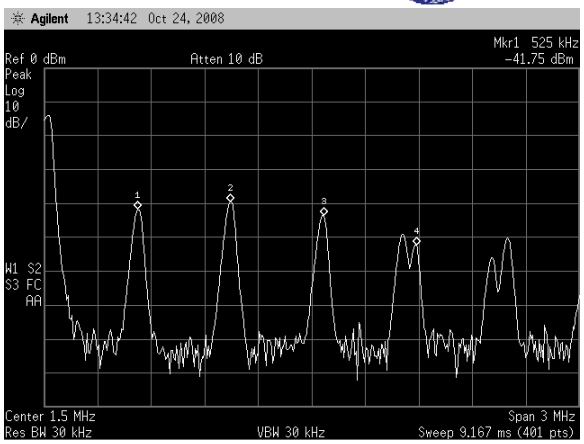

Figure 32 - Output with passive filtering.

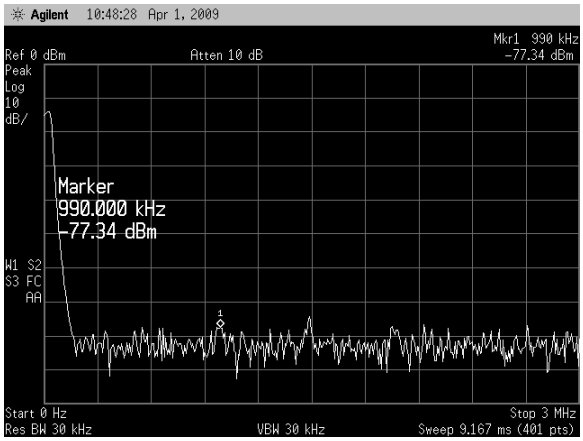

Figure 33 - Input with active filtering no –12-V.

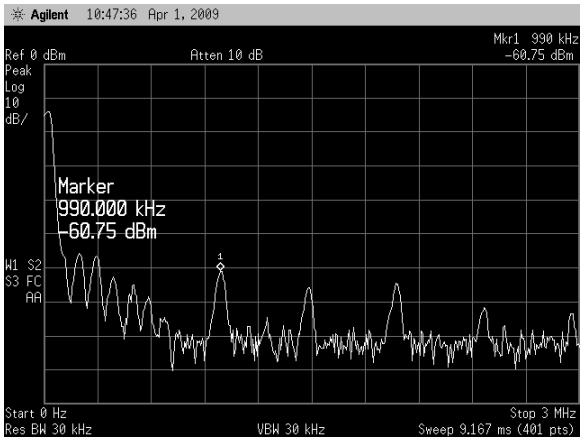

Figure 34 - Output with active filtering no –12-V.

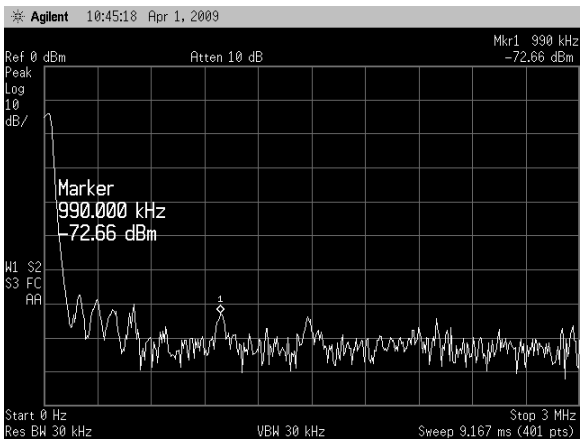

Figure 35 - Input filtering with –12-V.

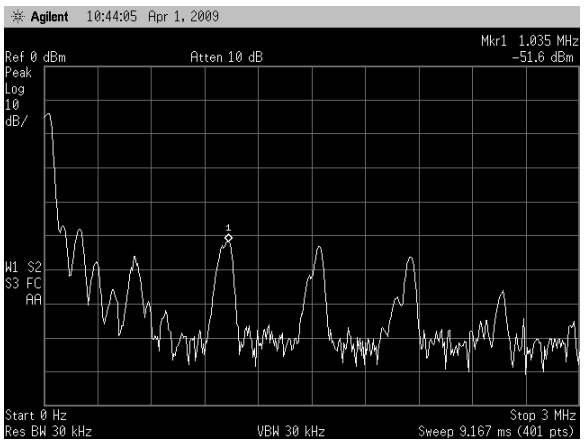

Figure 36 - Output filter with –12-V.

3.5 Mechanical Design

The spacecraft primary structure is composed of six panels to form a cube with the dimensions 22.31 × 22.31 × 18.95 inches. The mass of the spacecraft has a 50-kg constraint. Five of the six panels have an orthogrid pattern, and the bottom panel has a modified isogrid pattern. The bottom panel differs from the others because this panel acts as the launch vehicle interface. Solar panels are then attached to these panels to give the maximum area for solar power conversion. All components are attached to the internal walls of the panels. The structure is designed to have a factor of safety of at least 2.0. The design of the structure was planned to withstand a random vibration of 20 g's on each axis and a sine vibration with a fundamental frequency less than 100 Hz.

The finished fabricated product for the FCR included two side panels and all the internal components, except the boom. The bottom and one side panel were machined. The other four panels were made of polycarbonate plastic, which allowed for the internal components to be seen. The polycarbonate panels also provided the capability for a fit check. Figure 38 displays the final prototype.

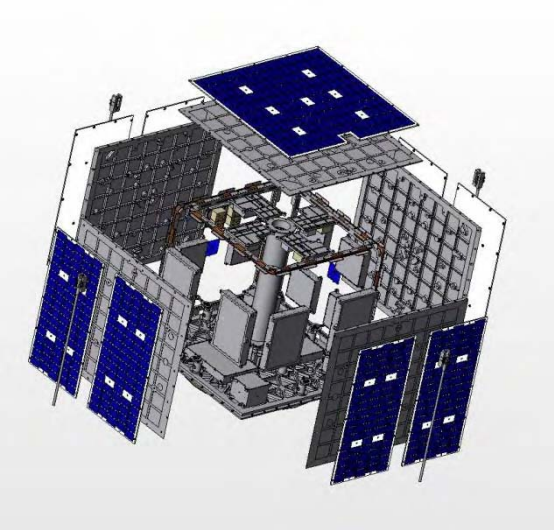

Figure 37 - NittanySat exploded view.

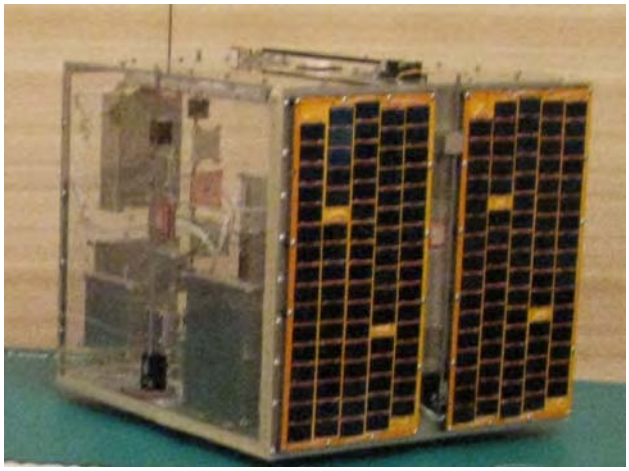

Figure 38 - NittanySat at FCR.

3.6 Command and Data Handling

The NittanySat flight computer will be a PC/104 form-factor computer manufactured by Arcom. The computer will consist of a CPU module and a serial interface module. A Flash disk-on-chip will hold an embedded version of the Linux Operating System as well as the mission's code.

To provide interface to the other systems on the satellite, the Emerald 8-port serial interface card will be used. The card, from Diamond Systems, provides eight (8) RS-232/422/485 serial ports with baud rates up to 115.2 kbps. Consistent with the PC/104 architecture, the card stacks with the Arcom CPU module. Linux drivers are provided to add support for the serial ports.

3.6.1 CDH Interface Diagram

The hardware and software interface diagrams are depicted in Figures 39 and 40, respectively, and the data volume budget is tabulated in Table 3.

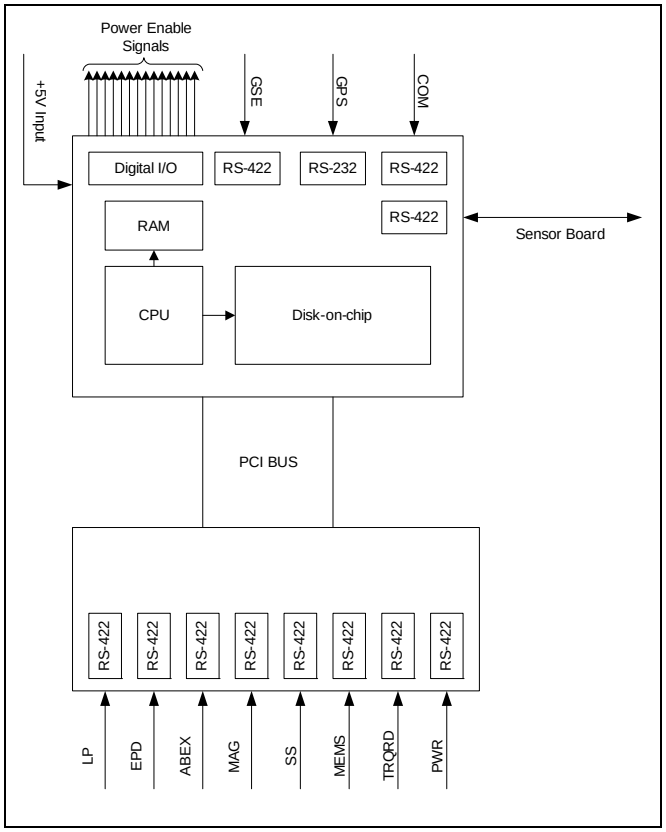

Figure 39 - CDH electrical interface diagram.

3.6.2 Software Interface Diagram

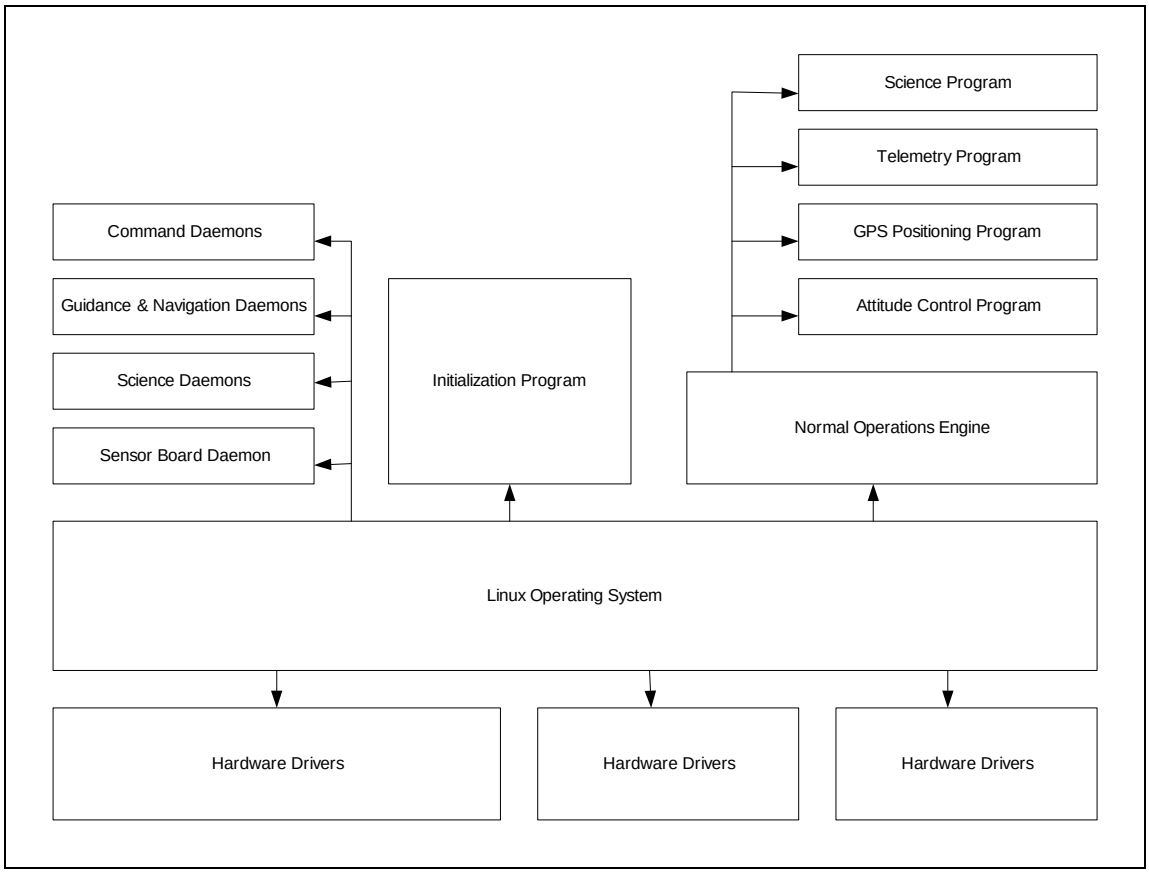

Figure 40 - CDH Software interface diagram.

3.6.3 Data Volume Budget

Table 3 - Data Volume Budget

Data Volume Budget		
Downlink Bandwidth	19200	bps
Uplink Bandwidth	19200	bps
Maximum Time between downlink pass	600	sec
Average Pass Length	600	sec
Maximum Time over science GS before PSU-GS * 3 passes at an average of 795 seconds per pass	600	sec
Science Data Rate	310	bps
Housekeeping Data Rate (MAX)	721	bps
Maximum Data Download = Downlink BW * Pass Length	11520000	bits
Maximum Science Data Accumulated	5616000	bits
Maximum Housekeeping Data Accumulated	1297800	bits
Minimum Housekeeping Data Per Pass	721	bits

3.7 Power System

The power system (PS) of NittanySat is being developed to provide the required power for the operation of all electrical systems on the spacecraft. The power system provides mission critical support, and therefore must be operational for the lifetime of NittanySat. The main objectives of the power system are to generate, distribute and store energy and be operational mode flexible for the functionality of NittanySat. The NittanySat power system utilizes similar designs as other nanosatellites. Power is converted from solar energy to a regulated DC bus. The PS Interface Diagram is depicted in Figure 41 and the power budget is tabulated in Table 4.

3.7.1 PS Interface Diagram

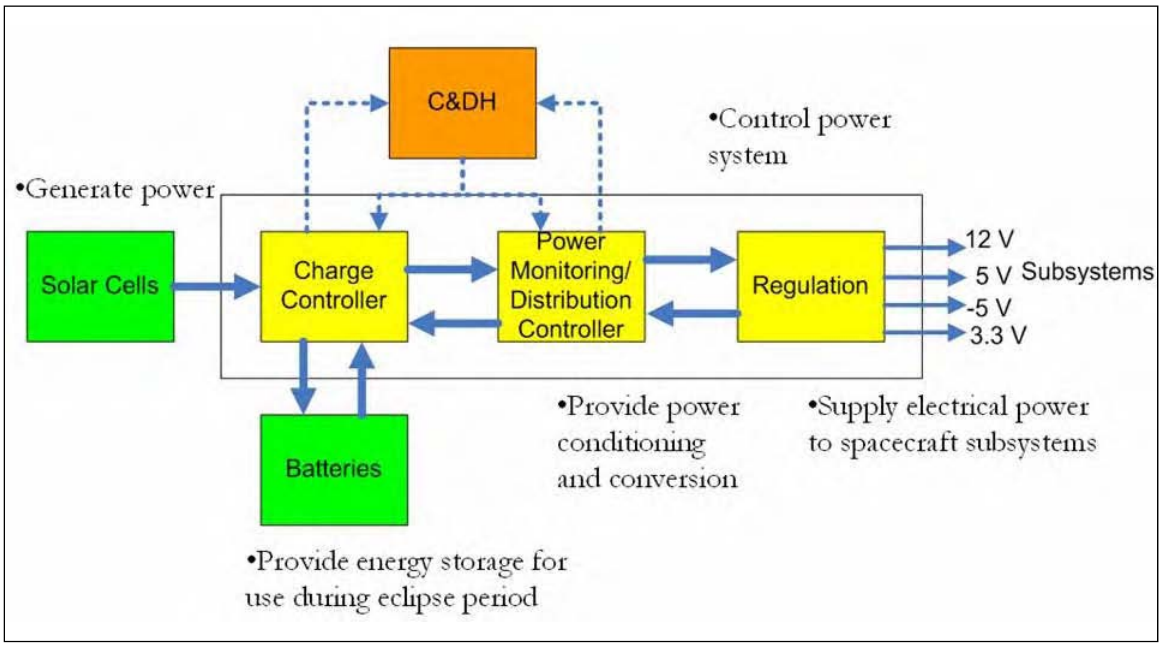

Figure 41 - PS interface diagram.

3.7.2 Power Budget

Table 4 - Power Budget

	Required Voltage (5,15)	Operating Current (mA)	Operating Power (W)	Normal Operating Modes (W)
PAYLOAD				
ABEX	5	150	0.75	0.75
ABEX LNAs (4)	15	264	3.96	3.96
Langmuir Probe (LP)	unregulated		2	2
LP Clean Operation (Only on once)	unregulated		0.25	
LP Boom Deployment (Once few sec)	unregulated		60	
EPD Circuitry	5	50	0.25	.25
Energetic Particle Detectors (2)	5	200	1	1
STRUCTURES				
Deployments (2 on at once)	24	300	7.2	
COMMUNICATION				
Transceiver (transmit)	5	500	2.5	2.5
Comm LNAs (1)	15	325	4.875	4.875
COMMAND AND DATA HANDLING				
Computer Board	5	1000	5	5
Sensor Board - 5V	5	100	0.5	0.5
GUIDANCE NAVIGATION AND CONTROL				
Magnetometer	15	35	0.525	0.525
Sun Sensors (5)	5	100	0.5	0.5
Magnetic Torquers	5	3000	15	
POWER				
Charger	16.8	1000	16.8	
Distribution	5	50	0.25	0.25
15% Regulation and Conversion loss			3.354	3.3165
THERMAL				
Heaters				
Total Required Power				25.426 Watts

3.7.3 PS Testing

Table 5 - Values from Test with Solar Simulator

Angle [Degrees]	Output Voltage [V]	%Voltage Drop	Current [A]	%Current Drop	Power [W]	%Power Drop
90	0.03	96.77	0.006	96.77	0.00018	99.90
80	0.33	64.52	0.066	64.52	0.02178	87.41
70	0.67	27.96	0.134	27.96	0.08978	48.10
60	0.89	4.30	0.178	4.30	0.15842	8.42
50	0.9	3.23	0.18	3.23	0.162	6.35
40	0.91	2.15	0.182	2.15	0.16562	4.25
30	0.92	1.08	0.184	1.08	0.16928	2.14
20	0.92	1.08	0.184	1.08	0.16928	2.14
10	0.92	1.08	0.184	1.08	0.16928	2.14
0 (Rays incident to cell)	0.93	0.00	0.186	0.00	0.17298	0.00

The MATLAB simulation program takes numbers from the table above and computes the maximum and minimum power from the solar cells. The solar cell simulation program discussed later, shows the power from the solar cells on the days of maximum and, minimum power.

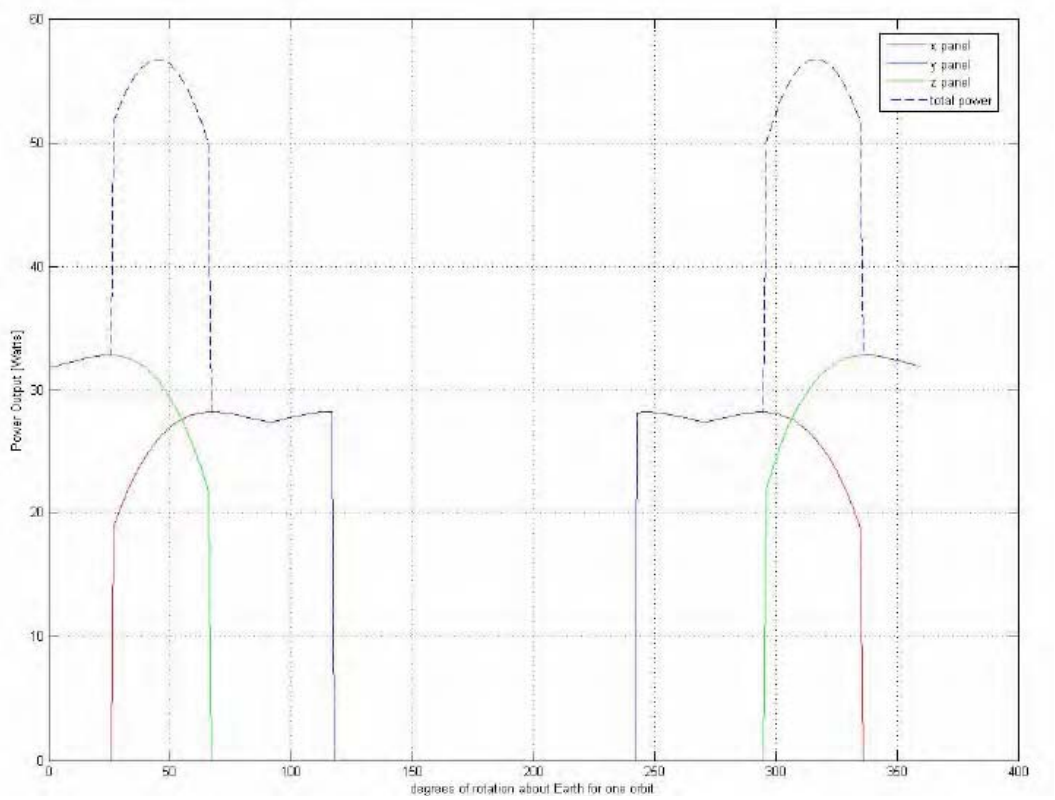

Figure 42 - Day 1 Simulation.

Figure 43 - Day 28 Simulation.

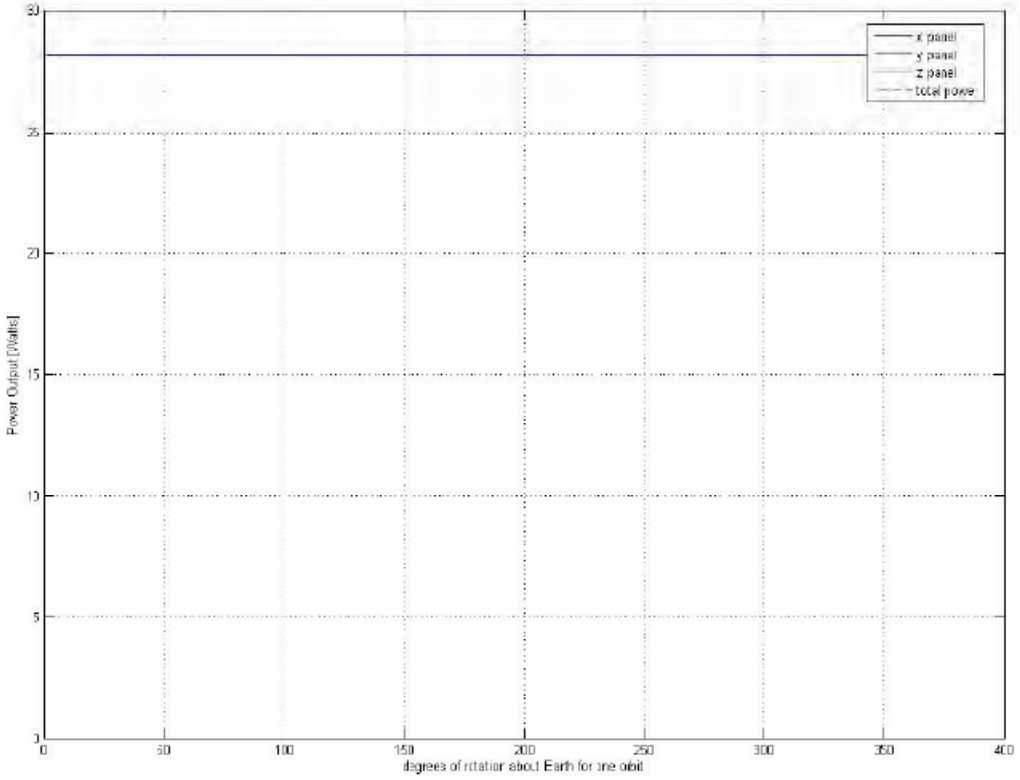

Figure 44 - Day 90 Simulation.

Figures 42 through 44 show that the minimum power that the satellite will output is roughly 27 watts, while the max power is roughly 74 watts. Day 1 and day 90 show roughly the minimum power output, while day 28 shows a spike in power. The spikes are attributed to multiple sides of the satellite in sunlight. From this simulation, the minimum power is being designed to and the maximum power is being taken into account. This simulation also shows that there is enough power for all the instruments on its day of least power. The power budget showed that 25.7 watts of power was needed for the satellite.

3.8 Guidance, Navigation, and Control

The Guidance, Navigation, and Control subsystem uses active and passive control techniques in order to stabilize the spacecraft. The design of NittanySat is to be gravity-gradient stabilized. During the initialization phase, the magnetic torque coils will be used to orient the payload. When current flows around the coil, a magnetic moment is generated that will orient the spacecraft along the local geomagnetic field. For feedback to create a closed loop control, a magnetometer and six solar sensors (one solar sensor per panel) will be used. For location information, NittanySat will have a GPS unit. Once NittanySat is in a preferred stable orientation, the gravity gradient boom will be deployed to act as passive stabilization. Figures 45 and 46 depict the magnetic torque coil and their placement on the structure. Figure 47 depicts the deployed gravity gradient probe.

Figure 45 - Single magnetic torque coil.

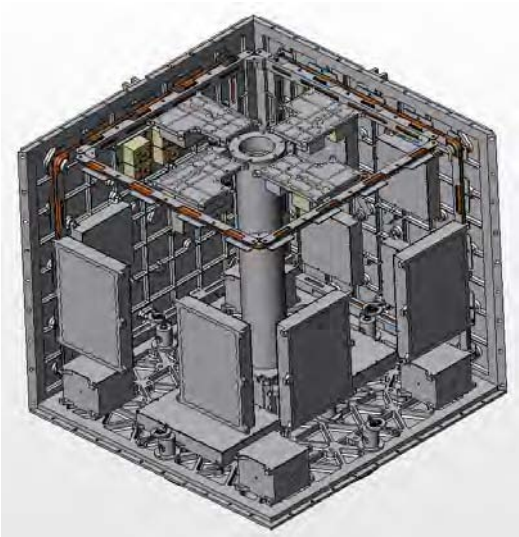

Figure 46 - Placement of magnetic torque coils with one coil per axis.

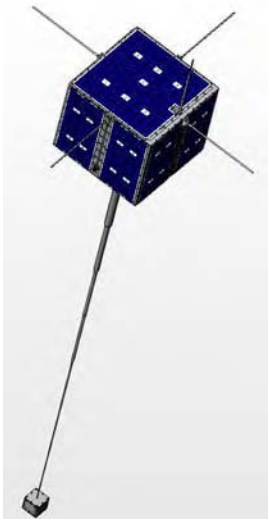

Figure 47 - NittanySat with gravity-gradient boom deployed.

3.9 Communications

The communications subsystem is required to downlink the data taken during flight and to receive any command uplinks from the ground station. The transceiver chosen is the MHX2420 from Microhard Systems. The antennas that are going to be used are patch antennas. The maximum data link rate is set to 19.2 kbps.

3.9.1 COM Link Budget

The link budget for NittanySat consists of values given by AGI's Satellite Toolkit. The tables below shows these values. Note that the budget constrains the values to the minimum BER as indicated by the requirement of a BER no greater than 1×10^{-06}. The elevation angle between the ground station and the satellite is no less than 10°.

Downlink Budget

Xmtr Power (dBW)	0
Xmtr Gain (dB)	1.3
EIRP (dBW)	1.3
Free Space Loss (dB)	-169.789
Atmos Loss (dB)	-0.6082
Rain Loss (dB)	-0.0751
TropoScintill Loss (dB)	-7.2429
Prop Loss (dB)	-177.715
Freq. Doppler Shift (KHz)	27.32082
Rcvd. Frequency (GHz)	2.450027
Rcvd. Iso. Power (dBW)	-176.415
Flux Density (dBW/m^2)	-147.176
Rcvr Gain (dB)	21.5561
Tequivalent (K)	290
g/T (dB/unitDegK)	-6.07822
C/No (dB*Hz)	53.88819
Bandwidth (KHz)	19.2
C/N (dB)	11.0552
Eb/No (dB)	14.0655
BER	2.21E-07

Uplink Budget

Xmtr Power (dBW)	10
Xmtr Gain (dB)	32
EIRP (dBW)	42
Free Space Loss (dB)	-171.266
Atmos Loss (dB)	-0.909
Rain Loss (dB)	-0.1278
TropoScintill Loss (dB)	-18.5977
Prop Loss (dB)	-190.901
Freq. Doppler Shift (KHz)	38.48974
Rcvd. Frequency (GHz)	2.450038
Rcvd. Iso. Power (dBW)	-148.901
Flux Density (dBW/m^2)	-119.662
Rcvr Gain (dB)	1.3
Tequivalent (K)	290
g/T (dB/unitDegK)	-26.3343
C/No (dB*Hz)	53.36405
Bandwidth (KHz)	19.2
C/N (dB)	10.531
Eb/No (dB)	13.5413
BER	9.97E-07

3.10 Thermal

The components of a satellite are constrained by a range of temperatures in which the systems can operate and survive. Therefore, the task of the thermal subsystem is to maintain the payload, solar panels, other subsystems, and the structural bus within these limits in order for the spacecraft to accomplish the mission goals. Various methods for achieving this can be utilized, but all can be placed into two categories: active or passive thermal control.

Active thermal control employs components such as heaters, mechanical/movable elements, and fluid-loop devices. In passive thermal control, no active components are used. Multilayer insulation (MLI), radiators, heat pipes, louvers, coatings/paints, and phase change devices can be used to modify the thermal performance of the spacecraft.

The thermal behavior of the satellite is result of the thermal inputs and the thermal properties of the vehicle components and structure. Thermal inputs include direct solar radiation, reflected (from the earth) solar radiation, and infrared radiation from the earth. Also, heat generated by electronics onboard the spacecraft must be taken into consideration. The thermal gradients exhibited throughout the spacecraft are a result of these inputs taken together with parameters such as the thermal capacity, conductivity, surface area, and surface properties (e.g., absorptivity, emissivity) of the various components.

In order to make predictions and guide design choices, an analytical model must first be developed. Typically, developing this model consist of two processes. First, the altitude and orientation (relative to the Earth and Sun) is determined. Then the environmental thermal inputs are estimated. This is called a *Geometric Mathematical Model (GMM)* (SMAD, 1999). Second, a thermal model of the spacecraft, called a *Thermal Mathematical Model (TMM),* is generated in order to determine the thermal behavior of the spacecraft (SMAD, 1999). Usually a lumped-parameter nodal analysis is utilized and incorporates the thermal-physical properties of the spacecraft and the results from the GMM.

Conduction and radiation are the only forms of energy transport present on orbit. These processes dictate how energy is transferred between the satellite and the sun, earth, and deep space. Additionally, they govern the transfer of energy within the spacecraft.

A lumped-parameter nodal–finite difference method was utilized in our analytical model. The MATLAB/Simulink environment was employed to develop a preliminary thermal model of the NittanySat. A more detailed model is under development in the same environment; however, other solutions (e.g., ANSYS, ABACUS) are being explored.

Based on first-order estimates of the range of temperatures encountered with a simplified model of the satellite, it is believed that a fully passive system consisting of coatings and insulations will be adequate in maintaining safe thermal conditions. This also appears to be supported by the experience of previous University Nanosat Program entries among other sources (SMAD, 1999). However, the deployment of Kapton encased resistive heaters is still possible if more detailed analysis and thermal testing shows that their inclusion is necessary or will increase safety margins.

As described in the precious section, the GMM calculates the environmental thermal inputs. Currently, this module is programmed for calculating thermal inputs for worst case, cold and hot orbits.

Case	Altitude	Inclination	Beta Angle
Worst Case, Cold	800 km	90°	27.32°
Worst Case, Hot	800 km	90°	0°

In estimating the thermal fluxes for the hot case it is important to realize that this is a steady state condition. Also, the flux on the side panels (3,4,5,6) is considered to be averaged evenly over each panel as a result of the slow "BBQ" roll the spacecraft undergoes around its Z-axis. The results of this preliminary model are shown below.

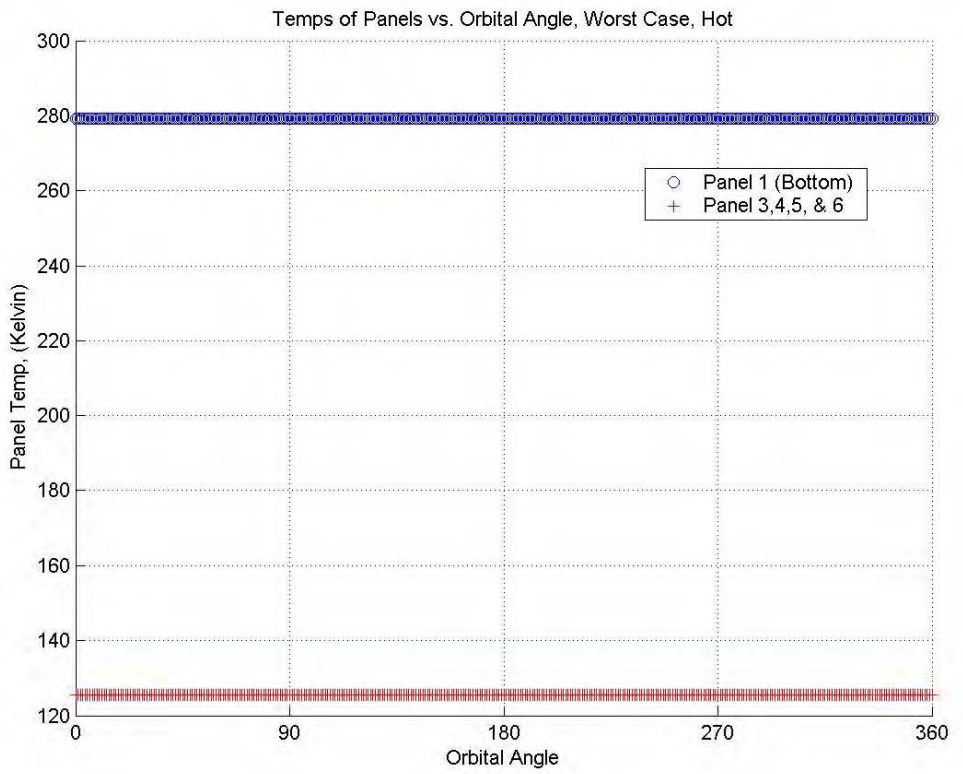

Figure 48 - GMM results for worst case, hot

It should be noted that panel 2 is not included as it is only exposed to deep space and any incident radiation (e.g., star shine, moon shine) is negligible.

Similarly, a GMM for the worst case, cold, case generates thermal flux inputs.

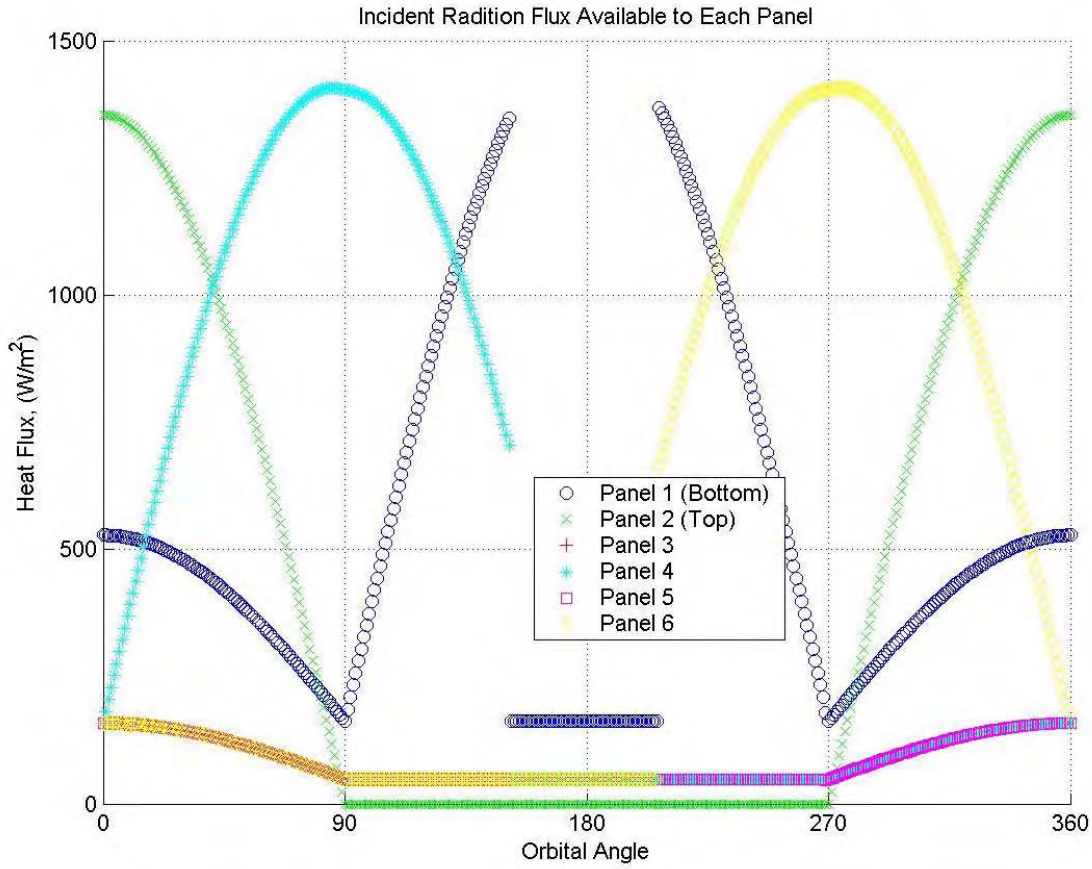

Figure 49 - GMM results for worst case, cold

The TMM, in its current state, is limited to 96 nodes (16 nodes per panel). It should be pointed out that the current models consist of components that are not coupled. In that, it does not produce "realistic" results. The current model's primary purpose is to demonstrate techniques and give the thermal subsystem group experience in modeling simple, if not high fidelity, scenarios.

A graph of the worst case, cold, is shown below. Notice that the deviation of the plots from their expected symmetry is due to "disturbance" cause by the initial temperature of the simulation. Future runs of the simulation will allow the temperature gradients to develop over additional orbits which will eliminate the effects of the initial temperature.

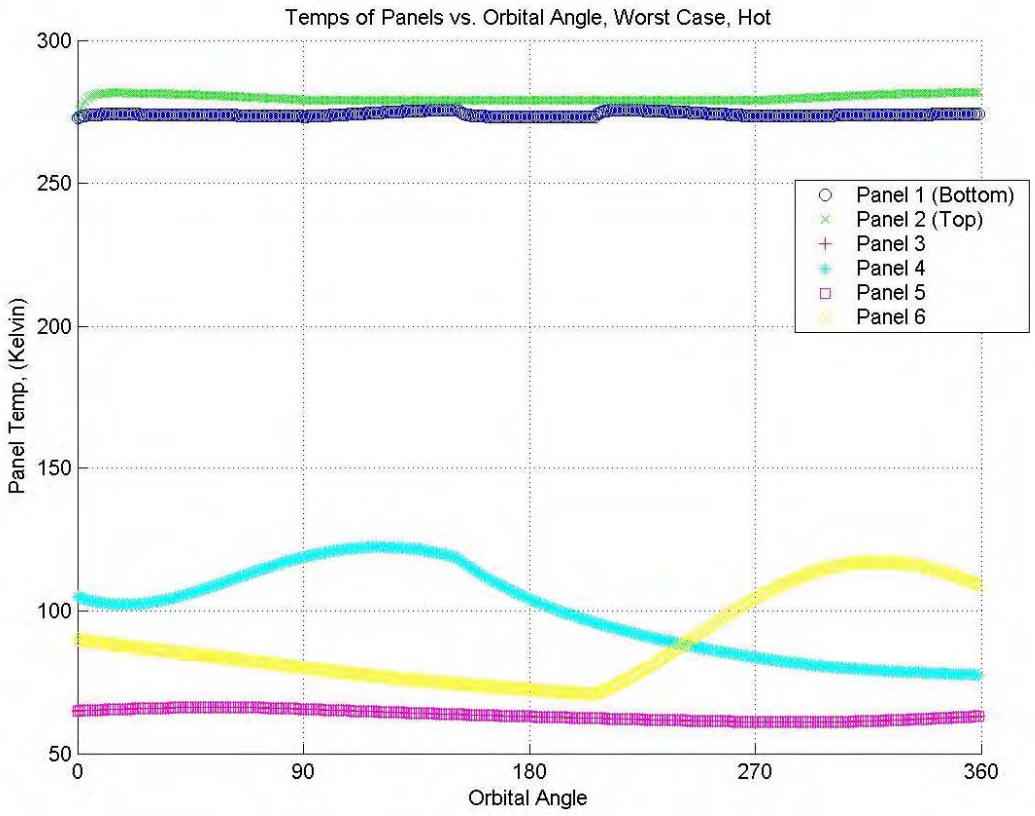

Figure 50 - TMM results for worst case, cold

Again, the results here are outside the range of expect results (specifically for panels 3,4,5,& 6) due to the fact that the model does not have thermally coupled panels. In addition, internal dissipation of the electrical systems is not included but will be included as part of the more detailed model currently under development.

4.0 Publications

Bilén, Sven G., C. Russell Philbrick, Adam C. Escobar, Brian C. Schratz, Eivind V. Thrane, Michael Gausa, Kolbjørn dahle, Farideh Honary, Steven Marple, Roger Smith, Martin Griedrich, and Thomas Zilaji. "NittanySat – A Student Satellite Mission for *D*-Region Study and Calibration of Riometers". Proceedings of the 18th ESA Symposium on European Rocket and Balloon Programmes and Related Research: Visby, Sweden. June 3–7, 2007. pp. 407–412.

Escobar, Adam and Sven G. Bilén. "Preliminary Design of the NittanySat Langmuir Probe Experiment". Annual Research Journal – Electrical Engineering Research Experience for Undergraduates. Department of Electrical Engineering, The Pennsylvania State University: University Park, PA. National Science Foundation Grant No. EEC-0244030. Vol. V. p. 51–58. 2007.

Wyant, Andrea, Adam Escobar, Perry Edwards, Sven Bilén, and Russell Philbrick, "Investigation of High Latitude D-Region Effects on RF Propagation," 12th International Ionospheric Effects Symposium, Alexandria, VA, 13–15 May 2008.

Schuette, Daniel, Adam C. Escobar, and Sven G. Bilén. "Circuit Design for NittanySat Solar Sensor". Annual Research Journal – Electrical Engineering Research Experience for Undergraduates. Department of Electrical Engineering, The Pennsylvania State University: University Park, PA. National Science Foundation Grant No. EEC-0244030. Vol. VI. p. 37. 2008.

Escobar, Adam, Sven G. Bilén, John D. Mitchell, and W. Kenneth Jenkins. A Langmuir Probe Instrument for Research in the Terrestrial Ionosphere. Thesis for Master of Science Degree. Department of Electrical Engineering, The Pennsylvania State University: University Park, PA. 2009.

5.0 New Discoveries

None.

6.0 Honors/A wards

Principal Investigator
Dr. Sven Bilén - 2008 Perez Memorial Student Advocate Award

7.0 Outreach

Engineering Open House
Various high school students from the state of Pennsylvania attended this event to learn more about educational and research opportunities at Penn State.

Space Day
Organized with the sponsorship of the Pennsylvania Space Grant Consortium, Space Day at Penn State included visitors from toddlers to adults.